4D Electron Microscopy Visualization of Anisotropic Atomic Motions in Carbon Nanotubes

Sang Tae Park, David J. Flannigan, and Ahmed H. Zewail*

Physical Biology Center for Ultrafast Science and Technology, Arthur Amos Noyes Laboratory of Chemical Physics, California Institute of Technology, Pasadena, California 91125, United States

ABSTRACT: We report the anisotropic atomic expansion dynamics of multi-walled carbon nanotubes, using 4D electron microscopy. From time-resolved diffraction on the picosecond to millisecond scale, following ultrafast heating at the rate of 10^{13} K/s, it is shown that nanotubes expand only in the radial (intertubule) direction, whereas no significant change is observed in the intratubular axial or equatorial dimensions. The non-equilibrium heating occurs on an ultrafast time scale, indicating that the anisotropy is the result of an efficient electron−lattice coupling and is maintained up to equilibration. The recovery time, which measures the heat dissipation rate for equilibration, was found to be on the order of $\sim 100~\mu$s. This recovery is reproduced theoretically by considering the composite specimen−substrate heat exchange.

Allotropes of carbon (e.g., C_{60}, graphene, and nanotubes) are some of the most intensely studied materials owing to their remarkable mechanical, electronic, and thermal properties.[1] The origin of these properties lies in the extended π-conjugation of the carbon network. The sp^2 hybridization of the carbon atoms imparts both very strong bonding, making for robust structures, and excellent charge-carrier and phonon transport due to very low scattering-center densities, especially in pristine specimens. In addition, ordered carbon materials are excellent candidates for fundamental studies of low-dimensional systems, with carbon nanotubes (CNTs) being quasi-one-dimensional and graphene purely two-dimensional.[2]

The structural and electronic properties of CNTs have been studied with a wide array of techniques. For example, ultrafast spectroscopic techniques have been used to probe the non-equilibrium dynamics of charge-carrier generation, transport, and decay in single- and multi-walled CNTs.[3,4] The time-dependent response of the carbon nuclei to external stimuli, however, remains an area of limited understanding. Indeed, techniques such as Raman spectroscopy provide information on specific vibrational modes,[5] but the positions of atoms comprising the lattice planes are not directly observable. Thus, without direct-imaging techniques having the proper spatiotemporal resolution, properties such as the relative changes in lattice spacing as a function of time, especially on the time scales associated with electron−phonon coupling and vibrational frequencies (~ 100 fs),[6−8] are not directly accessible.

Ultrafast electron microscopy (UEM), with its combined atomic-scale spatial and femtosecond to millisecond temporal resolutions, enables the direct probing of the rapid response of nuclei to structural perturbations.[9,10] This is achieved, in part, by using precisely timed electron packets to probe the structure. By delivering these electron packets to the specimen at precise times relative to an optical excitation pulse, electron−matter scattering theories can be applied to elucidate the ultrafast structural dynamics.

With UEM, here we report the anisotropic lattice dynamics of multi-walled carbon nanotubes (MWCNTs) on the picosecond to millisecond time scales. A picosecond laser pulse (2.33 eV to excite in the tail of π plasmon at ~ 5 eV[3,4]) excites the charge-carriers in the nanotubes which rapidly relax by scattering off the carbon nuclei, leading to a change in the lattice structure. These atomic-scale dynamics are elucidated by following the relative changes in the positions of the Debye−Scherrer rings observed in the UEM electron diffraction patterns. In this way, we are able to differentiate between the motions that occur along the nanotube radius (i.e., along the weakly bound π-stacking direction) and those that occur within the plane of the individual tubes (i.e., the covalently bonded network).

The diffraction patterns (Figure 1a), which were generated by selecting a specific region only with a post-specimen
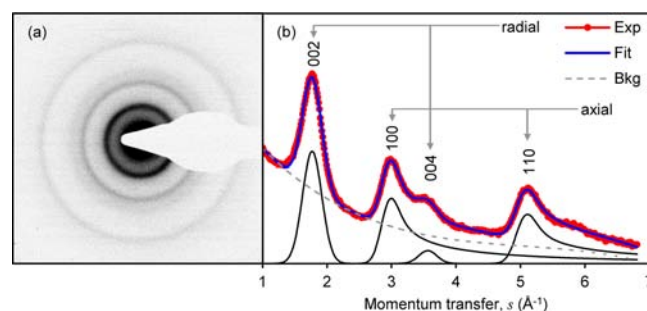

Figure 1. (a) Debye−Scherrer diffraction rings pattern and (b) angular-integrated 1D diffraction curve of MWCNTs in the ground state. Also shown are peak assignments, individual fitted profiles of symmetric and asymmetric peaks, and background.

aperture, consisted of Debye−Scherrer rings. This is because the specimen is a patch of randomly oriented MWCNTs supported by a lacey carbon substrate. The camera length was calibrated using standard aluminum powder diffraction. Two-dimensional diffraction patterns were subsequently angular-integrated to form a one-dimensional curve (Figure 1b), which was decomposed to background and diffraction peaks. The background due to diffuse scattering was fitted with a fourth-
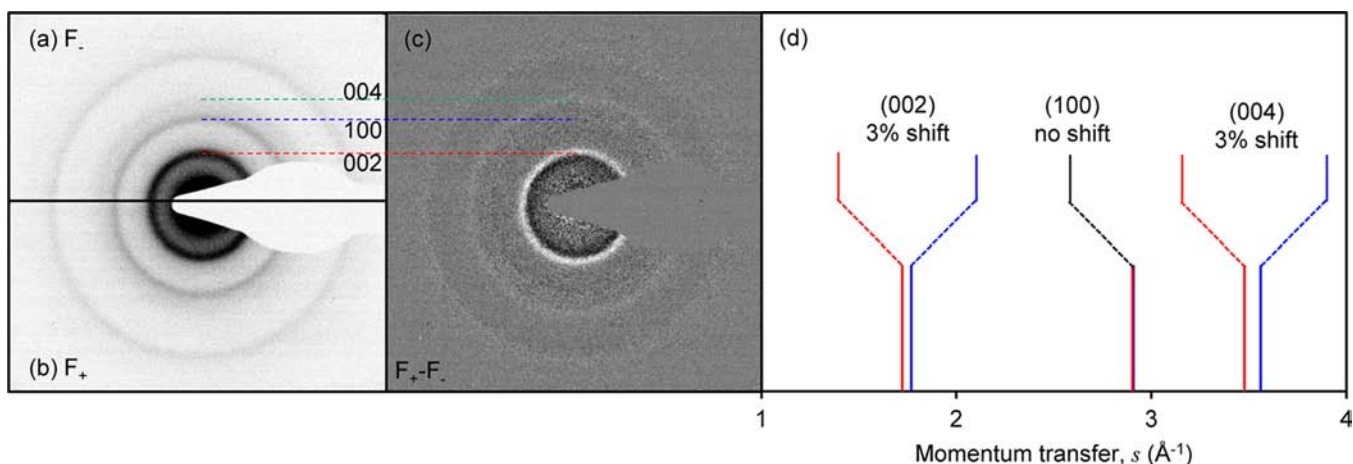
Figure 2. Diffraction frames (F) taken at negative and positive time: (a) −60 ps (F_−) and (b) +60 ps (F_+) with respect to the heating pulse. (c) Difference pattern between F_+ and F_− displaying the shifts observed for the (002) and (004) rings and the absence of the shift for the (100) ring. Bars in (d) indicate such shifts.

order polynomial. Gaussian profiles were used to determine the positions of the (002) and (004) peaks, which arise from scattering by the intertubule planes (van der Waals forces). Because of the asymmetric profiles of the (100) and (110) peaks, which correspond to the intratubule spacings (covalent bonding), a theoretical asymmetric peak profile was used for the fitting.[11] A typical convoluted fit of the calculated peak profiles to the MWCNT diffraction curve at the ground state is shown in Figure 1b. For the dynamics study, the diffraction patterns were recorded, and the individual diffraction peaks were analyzed as a function of the delay time between the heating pulse and the electron imaging pulse (Figure 2).

The temporal behavior of diffraction from picoseconds to milliseconds is shown in Figure 3. In order to gain access to such a wide temporal range, we used two distinct laser systems. For the studies spanning picoseconds to a few nanoseconds (Figure 3a), the frequency-doubled output (2.33 eV) of a picosecond laser [16 ps pulse-width (full width at half-maximum, fwhm) operated at a repetition rate of 1 kHz] was split into two beams. One of the beams was frequency-quadrupled to produce ultraviolet pulses (4.66 eV, 1.5 μJ/pulse), which were used to generate the probe photoelectron packets. The other beam was temporally delayed with a long-travel linear translation stage and used to excite the specimen at a fluence of ~50 mJ/cm². The 1 kHz repetition rate was chosen to ensure that the specimen completely relaxed before the next excitation pulse arrived (see Figure 3c). For the nanosecond experiments (Figure 3b,c), ultraviolet (4.66 eV, 2.8 μJ, 10 ns fwhm, 25 ns jitter) laser pulses were used to generate the photoelectron packets, while picosecond pulses from the same laser mentioned above were used to excite the specimen. The delay between the nanosecond photoelectron packets and picosecond optical excitation pulses was controlled with a digital delay generator, which was triggered with respect to the acousto-optic modulator divider synchronization output of the picosecond laser. By using the same pump laser for the picosecond and nanosecond experiments, any variations that would have been introduced by switching beams are eliminated, thus ensuring that the same structural dynamics are being excited and probed.

As can be seen in Figure 3, the lattice spacings of MWCNTs display a significant anisotropic response to laser heating: the (002) and (004) peaks instantly shift their positions, whereas the (100) and (110) peaks show virtually no change within our experimental/fitting error [note that any apparent changes observed in the (100) and (110) positions are attributed to a fitting error of the strongly overlapped peaks; see (100) in Figure 1b]. The normalized changes of the (002) and (004) peak positions are identical; the absolute shift scales appropriately with s, and the normalized values for both are the same. These results are consistent with the static X-ray diffraction experiments on MWCNTs, which showed no expansion in the intratubule lattice spacings up to 873 K.[12] Iijima and co-workers concluded that the geometry of MWCNT is that of a scroll of a single sheet, which can slightly unfold upon heating. Our results indicate that the same structure is robust in the non-equilibrium regime.

The observed lattice expansion in the quasi-equilibrium regime corresponds to a temperature rise of ~1000 K following the picosecond excitation, as determined from the ~3% expansion and using a thermal expansion coefficient of $\alpha_{00l} = 2.6 \times 10^{-5}$ K^{-1}.[12] From the fluence used to excite MWCNT (maximum ~3 μJ over ~75 μm diameter) and the absorption coefficient of amorphous carbon, $\alpha = 1.3 \times 10^5$ cm^{-1},[13] we obtained a temperature rise similar in magnitude to what has been observed. For the picosecond and early-stage nanosecond experiments (Figure 3a,b), no relaxation dynamics were observed up to 1 μs. In order to fully resolve the relaxation dynamics, time-scans up to 1 ms were performed (Figure 3c), and on these longer time scales, the diffraction slowly recovers to its pre-heating pattern.

Figure 4 shows the rise and decay of the temperature of the MWCNT, calculated from the diffraction. The rise time of the change in the (002) peak position is found to be response-limited (see Figure 4a), indicating an ultrafast anisotropic expansion of the MWCNT. The relaxation dynamics shown in Figure 3c deviate from a first-order exponential function. There may be several reasons for this: (1) the specimen rapidly reaches thermal equilibrium with the environment (i.e., substrate), the heat capacity of which is finite and is the rate-limiting system component for heat dissipation; (2) the specimen is inhomogeneous, consisting of a distribution of nanotube sizes with a range of structural defects that may exhibit different relaxation dynamics; (3) the structural dynamics result from non-thermal excitation and thermal relaxation. We can exclude the non-thermal excitation argu-
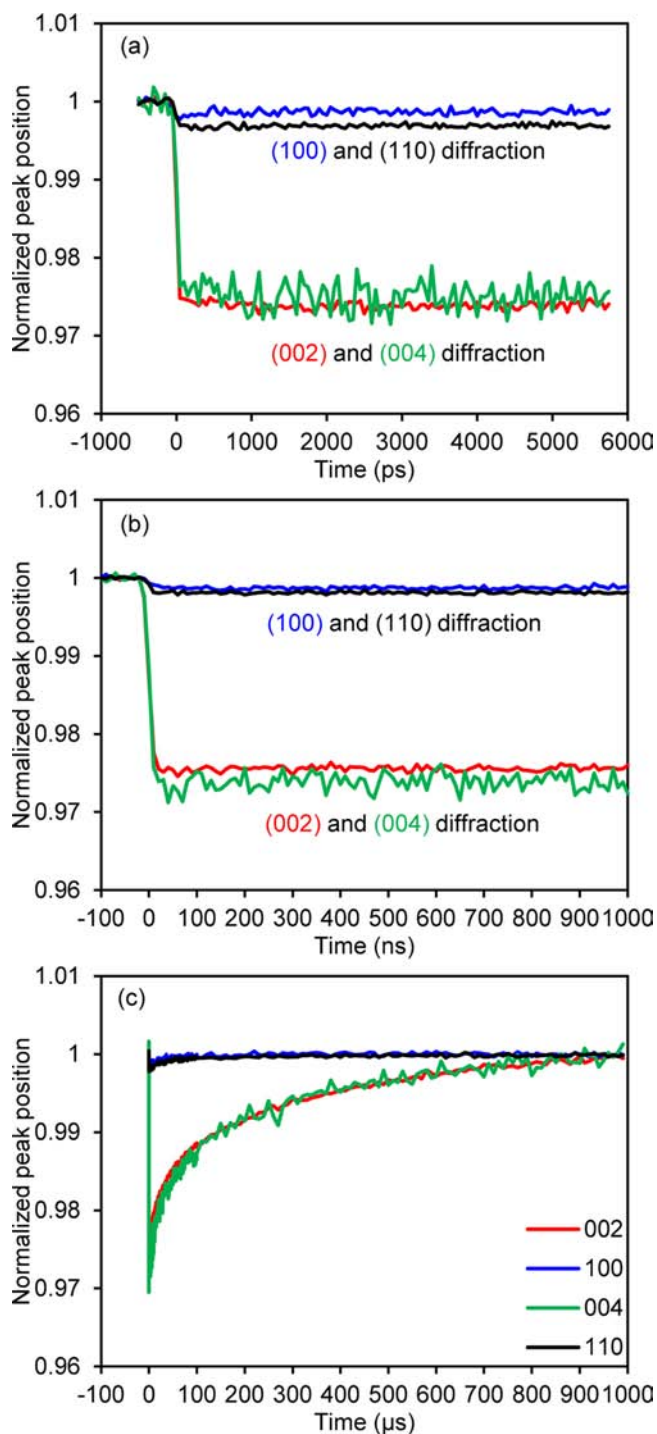
Figure 3. Temporal evolution of different diffraction-peak positions at (a) short, (b) intermediate, and (c) long time scale.

Figure 4. (a) Rise and (b) recovery dynamics of MWCNT/lacey carbon substrate/copper grid. The measured and fitted temperatures of MWCNT are shown in red and blue, respectively. The fitted temperature of the substrate is shown in black; the copper grid is at room temperature (see text). The inset shows a schematic geometry of nanotube specimen, substrate, and grid.

ment, because the relaxation time scale is on the order of 100 μs, and any electronic or coherent phonon process will decay within a picosecond. Because the specimen used in UEM studies has a significant thickness, thermal contact with the substrate is a dominant factor that will govern the heat dissipation kinetics. We considered a *simple* lateral (2D) diffusion. Although the result agrees with the early-time decay, it does not fit the transient at long times (>300 μs), due to the lack of a heat sink.

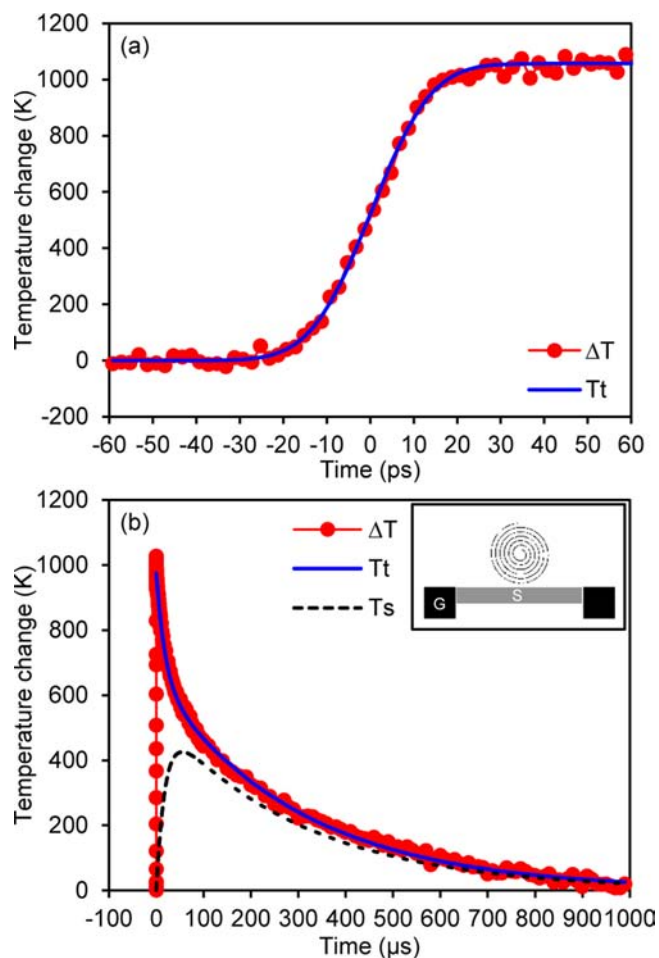Here, we instead invoke a *simple* model of heat conduction where the specimen is in thermal contact with the substrate, which in turn can dissipate the heat to a thermal reservoir (see Figure 4b inset) as follows:

$$T(T_t) \xrightarrow{k_1} S(T_s) \xrightarrow{k_2} G(T_g)$$

where T, S, and G stand for tube (CNT), substrate (lacey carbon), and grid bar (copper), respectively. In this case, T_g is the ambient temperature. By solving the kinetic equations, we obtained $(k_1)^{-1} = 48$ μs and $(k_2)^{-1} = 110$ μs, where k_i represents thermal conductance divided by heat capacity. Figure 4b shows the evolution of the temperature of the MWCNT specimen, compared to the fitted temperatures of CNT and substrate. Initially, CNT is instantly heated by the laser excitation, which in turn heats the substrate. Once CNT and substrate reach thermal equilibrium around 50 μs, the cooling dynamics is then governed by the slower heat dissipation to the copper grid.

In conclusion, the anisotropic atomic motions of multi-walled carbon nanotubes is directly visualized in the temporal profiles of their diffraction. The anisotropy of expansion reflects the nature of the bonding in the structures, which varies from strong covalent bonding to relatively weak van der Waals interactions. Our study revealed that the lattice expansion anisotropy is ultrafast at a heating rate of >10^{13} K/s, indicating

that electron–lattice coupling in such systems is indeed very efficient.[6−8] The results further indicate that the picosecond nanotube structure is scroll-type (see Figure 5) and is
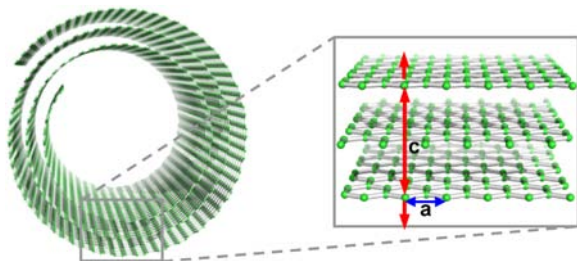

Figure 5. Schematic of MWCNT scroll and the anisotropic expansions.

maintained on the nanosecond and longer time scales. Thus, correlational studies between ultrafast imaging and atomic-scale diffraction with UEM can be performed to reveal the global mechanism of thermal and optomechanical motions,[14] with all motions resulting from initial picometer dynamics on the femtosecond time scale.

■ AUTHOR INFORMATION

Corresponding Author
zewail@caltech.edu

Notes
The authors declare no competing financial interest.

■ ACKNOWLEDGMENTS

■ REFERENCES

(1) *Carbon Nanotubes: Synthesis, Structure, Properties, and Applications*; Dresselhaus, M. S., Dresselhaus, G., Avouris, P., Eds.; Springer: New York, 2001; Vol. *80*.

(2) Geim, A. K. *Science* **2009**, *324*, 1530.

(3) Lauret, J. S.; Voisin, C.; Cassabois, G.; Delalande, C.; Roussignol, P.; Jost, O.; Capes, L. *Phys. Rev. Lett.* **2003**, *90*, 057404.

(4) Elim, H. I.; Ji, W.; Ma, G. H.; Lim, K. Y.; Sow, C. H.; Huan, C. H. A. *Appl. Phys. Lett.* **2004**, *85*, 1799.

(5) Dresselhaus, M. S.; Dresselhaus, G.; Saito, R.; Jorio, A. *Phys. Rep.-Rev. Sec. Phys. Lett.* **2005**, *409*, 47.

(6) Gambetta, A.; Manzoni, C.; Menna, E.; Meneghetti, M.; Cerullo, G.; Lanzani, G.; Tretiak, S.; Piryatinski, A.; Saxena, A.; Martin, R. L.; Bishop, A. R. *Nat. Phys.* **2006**, *2*, 515.

(7) Kato, K.; Ishioka, K.; Kitajima, M.; Tang, J.; Saito, R.; Petek, H. *Nano Lett.* **2008**, *8*, 3102.

(8) Lüer, L.; Gadermaier, C.; Crochet, J.; Hertel, T.; Brida, D.; Lanzani, G. *Phys. Rev. Lett.* **2009**, *102*, 127401.

(9) Zewail, A. H. *Science* **2010**, *328*, 187.

(10) Zewail, A. H.; Thomas, J. M. *4D Electron Microscopy: Imaging in Space and Time*; Imperial College Press: London, 2009.

(11) Yang, D.; Frindt, R. F. *J. Appl. Phys.* **1996**, *79*, 2376.

(12) Maniwa, Y.; Fujiwara, R.; Kira, H.; Tou, H.; Nishibori, E.; Takata, M.; Sakata, M.; Fujiwara, A.; Zhao, X. L.; Iijima, S.; Ando, Y. *Phys. Rev. B* **2001**, *64*, 073105.

(13) Hauser, J. J. *J. Non-Cryst. Solids* **1977**, *23*, 21.

(14) Flannigan, D. J.; Zewail, A. H. *Nano Lett.* **2010**, *10*, 1892.